Strain Energy Release Rate Distributions for Double Cantilever Beam Specimens

J. H. Crews Jr.,* K. N. Shivakumar,† and I. S. Raju‡
NASA Langley Research Center, Hampton, Virginia 23665

A three-dimensional finite element analysis was conducted for a double cantilever beam (DCB) specimen under mode I (opening) loading. The specimen had dimensions typical of 24-ply composite DCB test specimens. Strain energy release rate G distributions were calculated along a straight delamination starter for several different DCB materials. An isotropic DCB specimen was found to have a G distribution that varied significantly along its delamination front. This variation was explained as the combined result of the well-known boundary-layer effect and an effect due to anticlastic curvature of the bent specimen arms. The anticlastic curvature effects were discussed using the parameter $\nu_{xy} E_{yy}/E_{xx}$, where ν_{xy} is Poisson's ratio, and E_{xx} and E_{yy} are longitudinal and transverse (width-direction) moduli, respectively. This parameter was shown to be a good predictor of the G variability along the delamination front. A 0-deg graphite/epoxy specimen had a nearly uniform G distribution with a drop only near its edge, due to the boundary-layer effect. In contrast, a (±45 deg) graphite/epoxy case had a pronounced G variation across the specimen width. A bonded aluminum DCB specimen had a G variation that was nearly identical to a comparable specimen without a bondline.

Nomenclature

a	= delamination length
b	= specimen width
E_{al}	= Young's modulus for aluminum
E_{xx}	= Young's modulus in x direction
E_{yy}	= Young's modulus in y direction
G	= strain energy release rate
G_{Ic}	= mode I delamination fracture toughness
h	= thickness of each adherend
M_x	= moment producing σ_x stresses
M_y	= moment producing σ_y stresses
R	= radius of curvature
t	= half-thickness of midplane resin layer
w	= displacement in z direction
x,y,z	= Cartesian coordinates
ϵ_x, ϵ_y	= strain in x and y direction, respectively
ν_{xy}	= Poisson's ratio
$\sigma_x, \sigma_y, \sigma_z$	= stress in x, y, and z directions, respectively

Introduction

THE double cantilever beam (DCB) specimen (Fig. 1) is widely used to measure the mode I delamination fracture toughness of composite laminates and adhesively bonded joints. The change in the specimen's strain energy during delamination growth is computed to measure fracture toughness. Detailed stress analyses of the DCB specimen are needed to properly compute this strain energy release rate G. Several two-dimensional stress analyses of the DCB specimen have been presented; see, for example, Refs. 1 and 2. However, researchers have reported that delaminations in DCB specimens often grow with curved fronts rather than with a straight front, as assumed in two-dimensional analyses; see, for example, Refs. 3–5. Also, the delamination length-to-width ratio can cause errors in the calculation of G if the effect of finite width is not considered.[6] Furthermore, a recent three-dimensional stress analysis[7] showed that a straight delamination-starter insert has a variation of G along its length, with a pronounced drop near the specimen edges. The purpose of the present paper is to extend the three-dimensional stress analysis of the DCB specimen by computing G distributions along the delamination-starter front for several typical DCB specimens, and to use these results to analyze the parameters that influence this G distribution.

The variation of G along the DCB crack front is believed to be related to the anticlastic curvature[8] that can develop in the bent arms of the DCB specimen. This anticlastic curvature becomes a nonlinear phenomenon[8,9] at large bending moments. However, the present linear analysis is believed to apply to DCB specimens. The G distributions across the DCB specimen width were calculated by the three-dimensional virtual crack closure technique[10] with a three-dimensional finite element analysis like that in Ref. 7. Distributions are presented for DCB graphite/epoxy (G/E) specimens with the widely used 0-deg unidirectional layup and with a $(\pm 45 \text{ deg})_s$ layup, hereafter referred to simply as a ±45 deg layup. Similar G calculations were made for a bonded aluminum DCB specimen having an adhesive layer. An all-resin DCB specimen was also analyzed to provide an isotropic, monolithic reference case.

The G distributions are compared with one another and with similar distribution for an isotropic middle-crack specimen[11] that does not involve anticlastic curvature effects. Next,

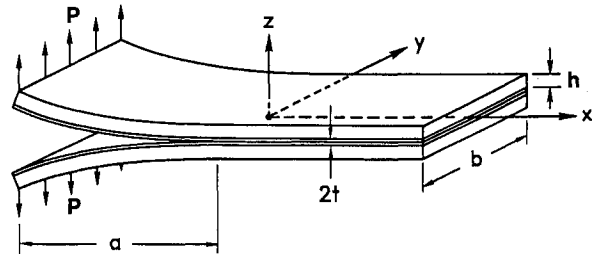

Fig. 1 DCB specimen configuration and loading.

Received March 14, 1990; presented at the AIAA/ASME/ASCE/AHS/ASC 31st Structures, Structural Dynamics and Materials Conference, Mobile, AL, April 3-5, 1990; revision received Sept. 24, 1990; accepted for publication Sept. 26, 1990.

*Senior Scientist.
†Senior Scientist, Analytical Services and Materials, Inc., 107 Research Drive, Hampton, VA 23666. Member AIAA.
‡Senior Scientist, Analytical Services and Materials Inc., 107 Research Drive, Hampton, VA 23666. Associate Fellow AIAA.

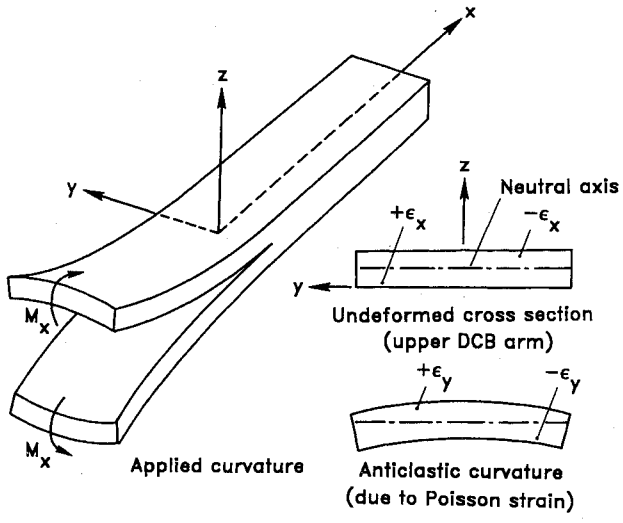

Fig. 2 Anticlastic curvature of DCB specimen arms.

different DCB cases are discussed in terms of their material properties that influence the G distributions. Finally, the G distributions are compared for a range of delamination lengths.

Loading and Anticlastic Curvature

For an applied bending moment M_x, as shown in Fig. 2, the bending strains ϵ_x produce Poisson's (transverse) strains ϵ_y that cause the specimen arms to develop transverse curvature. This anticlastic curvature is orthogonal to the applied curvature. A nonlinear analysis[8] of anticlastic curvature for an isotropic beam under pure bending explained the nonlinearity in terms of a transverse moment M_y that develops as a result of the anticlastic curvature of the beam's transverse section. This moment tends to counteract the anticlastic curvature as it develops. This behavior was discussed using the parameter b^2/Rh, where b is the beam width, R the applied radius of curvature, and h the beam thickness. In a DCB test, R is initially infinite and decreases as M_x increases from zero. For a given configuration, b^2/Rh increases linearly with M_x. Results in Ref. 8 for very small b^2/Rh values show that the beam's transverse section has "pure" anticlastic curvature with radius R/ν_{xy}, where ν_{xy} is Poisson's ratio. With increased bending, for $b^2/Rh > 6$, the transverse curvature was said to be "neutralized" and existed only near the beam's edges.

To put this nonlinear behavior in perspective for the present study, b^2/Rh was calculated for interlaminar fracture toughness G_{Ic} typical of a tough thermoplastic laminate of graphite/PEEK (APC-2).[12] Even for this rather extreme case ($G_{Ic} = 1230$ J/m^2), the maximum b^2/Rh value was < 2, suggesting that the anticlastic curvature behavior of DCB specimens may not be severely modified by the nonlinear neutralizing moment. Furthermore, at the delamination front where G is calculated, anticlastic curvature is prevented because the two halves of the specimen constrain each other. As a result, the G distributions are believed to be influenced by the specimen's tendency to develop anticlastic curvature and its corresponding resistance to such curvature, rather than the actual development of this curvature at the delamination front. Since anticlastic curvature is prevented at the delamination front, the neutralizing moment that produces the nonlinear behavior is also prevented. Consequently, the present linear analysis should produce reasonably accurate G calculations, even though it does not account for nonlinear anticlastic curvature in the DCB specimen arms.

A uniform displacement in the z direction was imposed at the end of the DCB arm, and the computed results were normalized by the resulting end load to obtain the unit-load (1 N/m) solution. This end loading should be a good approximation to usual DCB test conditions involving bonded loading hinges or tabs. Such hinges and tabs prevent anticlastic curvature at the end of the DCB specimen and, therefore, can influence the conditions along the delamination front, especially for short delamination lengths. This matter will be discussed.

Specimen Analysis Procedures

The DCB specimen analyzed in this study is shown in Fig. 1. The dimensions for this 24-ply split-laminate specimen ($b = 25$ mm and $h = 1.65$ mm) were selected to be typical of test specimens currently used. A range of delamination lengths from 6.35 to 200 mm was analyzed. For the two graphite/epoxy cases (0 and ± 45 deg layups), the resin-rich layer $2t$ was 0.01 mm thick, which is typical of cocured laminates. For the bonded aluminum DCB, this thickness was 0.1 mm, to represent an adhesive bondline. The material properties used in this study are presented in Table 1 and will be discussed when results are presented for each case.

The three-dimensional finite element model used in this study represented one-fourth of a 24-ply DCB specimen, as shown in Fig. 3. This model has the dimensions given in Fig. 1, and is identical to that used in Ref. 7. The modeling in the $y = 0$ plane has high mesh refinement near the delamination front, and is the same as that used in the two-dimensional analysis in Ref. 2. This two-dimensional model gave strain energy release rates within 1% of classical and other finite element solutions. The corresponding three-dimensional model was created by translating the two-dimensional model in the y direction. A convergence analysis[7] showed that a six-layer three-dimensional model had adequate refinement to compute the rather steep G distributions that were found near the specimen edge. This six-layer model had 20-noded isoparametric parabolic elements everywhere except along the delamination front, where collapsed elements were used within the thin resin layer, as shown. A total of 2808 elements, 13,569 nodes, and 40,707 degrees of freedom were used. A G value was calculated for each element along the delamination front, using the three-dimensional virtual crack closure technique introduced in Ref. 7 and explained in more detail in Ref. 10.

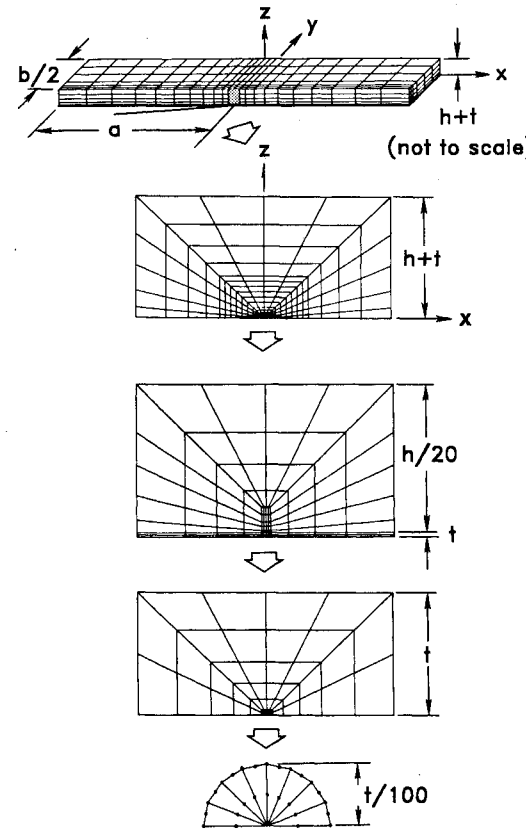

Fig. 3 Finite element model for the DCB specimen.

These G calculations involve products of opening forces ahead of the front and opening displacements behind it.

Results and Discussion

The results from this study are presented in three parts. First, the behavior of an isotropic (all-resin) DCB specimen is compared with an isotropic middle-crack (MC) specimen[11] to analyze the influence of bending on the G distribution in the DCB specimen. Next, two graphite/epoxy DCB specimens are analyzed to discuss the effects of their elastic properties on the G distributions. Also, a bonded aluminum adherend DCB specimen is analyzed and then compared with results for two cases with "modified" adherend properties. Finally, the effects of delamination length are discussed.

Bending Effects

Figure 4 shows the computed G distribution along the isotropic DCB crack front for a delamination length of 50 mm. To simplify comparisons among the various DCB cases analyzed, the G values in Fig. 4 have been normalized by their average along the crack front. The G averages are presented in Table 2. The G distribution for the MC specimen was taken from Ref. 11 which used finite element modeling and procedures similar to the present study. Also, the MC specimen had a crack length that was twice its thickness, comparable to the present DCB case. The G distribution for the MC specimen in Fig. 4 is nearly uniform along most of the crack front but drops by about 50% in a "boundary layer" equal to about 10% of the specimen thickness. This boundary-layer behavior was first reported in Ref. 13 and more recently has been analyzed by several researchers (see, for example, Refs. 14 or 15). In Refs. 11 and 16, this boundary-layer effect was shown to depend on Poisson's ratio, being more pronounced for higher ratios and nonexistent for a zero value. (A Poisson's ratio of 0.3 was used for both isotropic specimens in Fig. 4.)

In contrast to the isotropic MC specimen, the isotropic DCB specimen has a G distribution in Fig. 4 that varies all along the delamination front. In fact, this G curve drops to zero near the specimen edge. Because G is a function of the product of crack opening displacement and crack tip forces, this DCB curve can be better understood by examining the opening displacements and stresses near the delamination front. Figure 5 shows the distributions of opening displacement at a small distance (0.01 mm) behind the delamination front. In contrast to the nearly uniform distribution for the MC specimen, the DCB curve drops to zero near the specimen edge. This shows that the delamination does not open at the edge when the specimen is loaded. In fact, the opening displacement was computed to be slightly negative at the edge because the finite element analysis did not prevent "interpenetration" of the two delamination faces.

Table 1 Elastic material properties

	Resin	Aluminum	0-deg G/E	±45-deg G/E
E_{xx}, GPa	3.4	71.0	134	22.0
E_{yy}, GPa	3.4	71.0	13.0	22.0
E_{zz}, GPa	3.4	71.0	13.0	14.3
ν_{xy}	0.30	0.30	0.34	0.716
ν_{yz}	0.30	0.30	0.35	0.118
ν_{xz}	0.30	0.30	0.34	0.118
G_{xy}, GPa	1.3	27.3	6.4	34.2
G_{yz}, GPa	1.3	27.3	4.8	5.6
G_{zx}, GPa	1.3	27.3	6.4	5.6

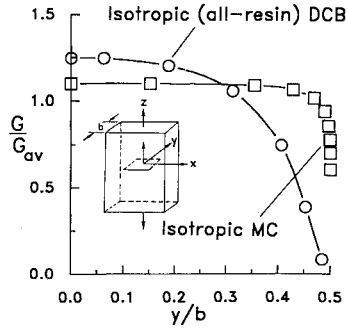

Fig. 4 G distributions for isotropic DCB and MC specimens.

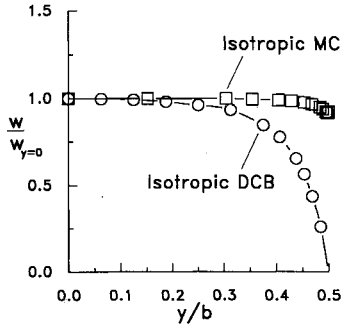

Fig. 5 Crack opening displacements for isotropic DCB and MC specimens.

Figure 6 shows the distribution of opening stress (σ_z) at a distance of 0.01 mm ahead of the delamination front. The stress distribution for the DCB specimen is similar to its displacement distribution and, again, its variation along the front is more pronounced than for the MC specimen. The DCB curves in Figs. 5 and 6 show that drops in the opening displacement and stress curves both contribute to the near zero G value shown at the DCB specimen edge in Fig. 4. Furthermore, the general variation of G along the delamination front for the DCB specimen appears to be the combined result of the well-known boundary-layer effect and anticlastic curvature due to bending in the DCB specimen arms.

Material Property Effects

Although the two arms of the DCB specimen tend to develop anticlastic curvature as they bend under an applied moment M_x, at the delamination front they are attached to one another and, therefore, resist this curvature. This midplane interaction between the two DCB arms causes a variation in the σ_z distribution across the specimen width. The σ_z variation at the specimen midplane produces a resisting moment M_y on each half of the specimen. By setting the anticlastic curvature equal to zero at the delamination front, moment-curvature relationships from plate theory lead to

$$M_y = (\nu_{xy}E_{yy}/E_{xx})M_x \tag{1}$$

Because M_y is related to the variation of σ_z across the specimen width and σ_z at the delamination front influences G, the M_y and the G distribution are, therefore, related. As a result, conditions that produce large M_y values from Eq. (1) should also produce large variations of G along the delamination

Table 2 Computed results for DCB specimens

	Isotropic[a]	0-deg G/E	±45-deg G/E	Aluminum adherend	Modified adherend 1[b]	Modified adherend 2[c]
$G_{av}(10^{-4}$ J/m$^2)$	20.2	0.572	2.54	1.00	0.110	1.05
$\nu_{xy}E_{yy}/E_{xx}$	0.300	0.033	0.716	0.300	0.030	0.030

[a]Resin properties used. [b]$E_{xx} = 10E_{al}$. [c]$E_{yy} = 0.1\ E_{al}$.

Table 3 Average strain energy release rates for 0-deg G/E DCB specimens

	a, mm					
	6.35	12.7	25.4	50.8	102	203
G_{av} (10^{-4} J/m^2)	0.0177	0.0496	0.162	0.572	2.20	8.77

front. As expected, Eq. (1) shows that ν_{xy} should influence the G distribution. However, the equation suggests that E_{xx} and E_{yy} can also be influential. The remainder of this section will focus on the effects of ν_{xy}, E_{xx}, and E_{yy} on G distributions. Note that $\nu_{xy}E_{yy}/E_{xx} = \nu_{yx}$ and, therefore, the present discussion could be simplified by using ν_{yx}. However, each of the material properties ν_{xy}, E_{xx}, and E_{yy} can have different contributions and will therefore be discussed individually.

Note that M_x is constant, because a 1 N/m loading was used throughout this study, and in this section, a single crack length (50 mm) was used. Because M_x is constant, all cases analyzed have the same bending stresses σ_x in the specimen arms. However, cases with different E_{xx} values have different bending strains ϵ_x and, therefore, different transverse strains ϵ_y. The corresponding differences in anticlastic (transverse) curvature influence the G distributions. The relevance of E_{yy} in Eq. (1) is its influence on the resisting moment needed to prevent anticlastic curvature along the crack front.

Graphite/Epoxy Specimens

Results for a 0-deg G/E DCB specimen are shown in Fig. 7. Compared to the G distribution for the isotropic (all-resin) DCB specimen, the 0-deg specimen has a much flatter curve. As shown in Table 1, these two specimens have nearly equal Poisson's ratios. But their E_{xx} moduli differ by a factor of about 40 (134.4 GPa for the 0-deg G/E case compared to 3.4 GPa for the isotropic case). When E_{yy} is also considered and the parameter ($\nu_{xy}E_{yy}/E_{xx}$) from Eq. (1) is computed, its value of 0.033 for the 0-deg case is about one-tenth the 0.300 for the isotropic case (see Table 2). Therefore, the finite element based curves in Fig. 7 agree qualitatively with the trend predicted by Eq. (1). In fact, the anticlastic curvature effect may not be important for the 0-deg G/E case. Comparison of this curve with the MC curve in Fig. 4 suggests that the drop in this G curve is due mostly to the boundary-layer effect. Figure 7 also shows the G distribution for the ±45-deg G/E DCB specimen. Because of the large Poisson's ratio for this case, the ν_{xy} E_{yy}/E_{xx} parameter is 0.716, which is more than twice that for the isotropic case. Accordingly, the ±45-deg curve in Fig. 7 shows a more pronounced G variation than the isotropic curve.

The G distribution for the ±45-deg case drops to zero beyond y/b = 0.45, which corresponds to about 10% of the specimen width. The present analysis allowed the two delamination faces to interpenetrate in this region. An effort was made to model this as a contact problem, using nodal constraints to prevent negative displacements. Unfortunately, the present finite element model was not developed with this problem in mind and, therefore, did not have adequate mesh refinement behind the delamination front. This contact problem requires additional study.

The larger G value toward the middle of the specimen suggests that delamination growth from a straight delamination-starter insert will occur first near the middle of the specimen. Also, because the delamination starter does not open near the specimen edge for the ±45-deg case, delamination growth should be delayed there. Because delamination lengths are usually measured by observing the specimen edges, such variations in delamination initiation could be troublesome when computing G_{Ic} for the first increment of delamination growth. When DCB delaminations grow, they can develop a curved front and, as expected from Fig. 7, more curvature has been observed for the ±45-deg case than for the 0-deg case.[4] Furthermore, recently published results[6] suggest that this curvature will change as the delamination grows in the ±45-deg DCB specimen.

Bonded Specimens

The G distribution for a bonded aluminum DCB specimen is shown in Fig. 8. Despite the presence of the 0.1-mm

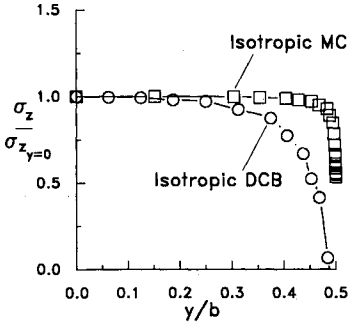

Fig. 6 Stress distributions for isotropic DCB and MC specimens.

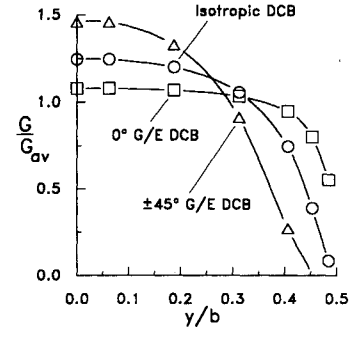

Fig. 7 G distributions for G/E DCB specimens.

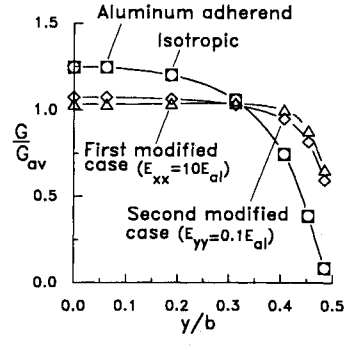

Fig. 8 G distributions for bonded DCB specimens.

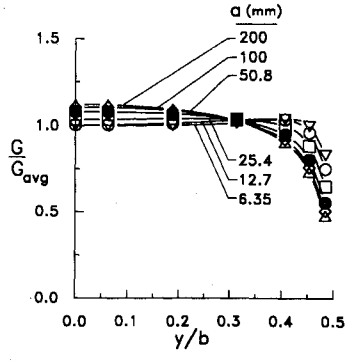

Fig. 9 G distributions for 0-deg G/E DCB specimens having a range of delamination lengths.

bondline, the curve for the aluminum adherend DCB (circular symbols) is virtually identical to that for the isotropic (all-resin) DBC specimen (square symbols). This behavior can be predicted from $\nu_{xy}E_{yy}/E_{xx}$ because it reduces to ν_{xy} for both of these cases; Table 1 shows that both cases have the same value for ν_{xy}. In Ref. 17, it was suggested that bonded metallic DCB specimens and composite DCB specimens could have these G_{Ic} if the same polymer were used as the adhesive in one case and as the matrix in the other. If this were true, small experimental quantities of polymers could be tested in bonded DCB specimens. Furthermore, this approach would eliminate the fiber bridging problems that can complicate composite DCB tests. However, the present study shows that bonded metallic DCB specimens and composite DCB specimens can have quite different G distributions. This difference could influence G_{Ic} measurements.

To explore the effects that E_{xx} and E_{yy} have on G distributions further, two modified adherend cases were analyzed. For the first such case, the aluminum adherend DCB was recalculated using an E_{xx} value that was 10 times the aluminum modulus (E_{al}) and all other properties were unchanged. This increase in E_{xx} decreased the bending strains ϵ_x, which in turn decreased the transverse strains ϵ_y, and, therefore, decreased the anticlastic curvature compared to the aluminum case. As expected, Fig. 8 shows that the G variation along the delamination front is less pronounced than for the aluminum adherend case. For this modified adherend case, the $\nu_{xy}E_{yy}/E_{xx}$ parameter was reduced from 0.30 to 0.030.

For the second modified case, the aluminum adhered DCB was reanalyzed using an E_{yy}, which was only one-tenth E_{al}. The E_{xx} was equal to E_{al}, and again the other properties were unchanged. As previously discussed, the relevance of E_{yy} is its influence on the resisting moment needed to prevent anticlastic curvature where the specimen halves are connected. The $\nu_{xy}E_{yy}/E_{xx}$ parameter equaled 0.030, as in the first modified case. As a result, the curves in Fig. 8 for the two modified cases are nearly identical, despite the fundamental differences in material properties for the two cases, This illustrates the value of this parameter in the analysis of anticlastic curvature effects on G distributions for DCB specimens.

Delamination Length Effects

The G calculations for the the 0-deg cases were repeated for a range of delamination lengths. The purpose of these calculations was to study the variation of anticlastic curvature effects with a, for different delamination starter lengths. Results are shown in Fig. 9 for a ranging from 6.35 to 200 mm. The corresponding average G values are presented in Table 3. The filled circular symbols in Fig. 9 represent the previous case with a = 50 mm, which is replotted from Fig. 7. The case with the shortest a (6.35 mm) had the least variation of G across the specimen width. Recall that the DCB specimen model was loaded by an imposed uniform displacement, which prevents anticlastic curvature at the end of the specimen arms. Also, as previously discussed, the interaction between the two specimen arms prevents anticlastic curvature at the delamination front. As a result, for this a = 6.35 mm case, the drop in G near the specimen edge is probably mostly due to the boundary-layer effect rather than the anticlastic curvature. This suggests that testing problems caused by the variation of G across the specimen width could be minimized by using a short delamination starter length and measuring the toughness with the first increment of growth.

For larger delamination lengths, more G variability occurs across the specimen width; however, this variability appears to approach a limiting condition. This suggests that as a delamination grows from a short straight delamination starter in a DCB specimen, the delamination front will gradually develop curvature but will eventually reach a stabilized shape. Conversely, these results suggest that if a sufficiently long delamination starter is used, the delamination front should quickly achieve a stabilized shape as the delamination grows. Therefore, some of the testing complications associated with the changing shape of the delamination front may be avoided by using long delamination starters.

Concluding Remarks

A three-dimensional finite element analysis has been conducted for a DCB specimen under mode I (opening) loading. The specimen had dimensions typical of 24-ply composite DCB specimens. Strain energy release rate G distributions were calculated along a straight delamination starter. The material properties represented an isotropic reference case, typical orthotropic graphite/epoxy laminates, adhesively bonded aluminum, and two special adherend cases.

The isotropic DCB specimen had a G distribution that varied all along its delamination front. This large G variation was attributed to the combined result of the well-known boundary-layer effect and an effect due to the anticlastic curvature caused by bending in the specimen arms.

The 0-deg graphite/epoxy case had a nearly uniform G distribution across most of the specimen width, with a drop occurring only within about 20% of the edge, probably attributable mostly to the boundary-layer effect. In contrast, the ±45-deg graphite/epoxy case had a pronounced G variation across the specimen width. Also, for the ±45-deg case the delamination did not open in a region very near the specimen edge. These results are consistent with observations of curved delamination fronts reported in the literature. The bonded aluminum DCB specimen had a G distribution that varied significantly but was shown to be nearly identical to a comparable specimen without a bondline.

The effects of anticlastic curvature on the G distribution were discussed using the parameter $\nu_{xy}E_{yy}/E_{xx}$ where ν_{xy} is the transverse Poisson's ratio, E_{xx} and E_{yy} are longitudinal and transverse (width-direction) moduli, respectively. Comparison of G distributions for the different cases with the same crack length showed that this parameter was a qualitative predictor of the degree by which G varied along the delamination front.

For very short delamination lengths, G for the 0-deg case had its least variation and this variation was believed to be caused by the boundary-layer effect. For larger delamination lengths, the G variations increased but approached a limiting shape. This suggests that some of the delamination test problems caused by the variation of G can be minimized by using a very short or a sufficiently long delamination starter.

The present exploratory study illustrates the importance of anticlastic curvature effects on G distributions for DCB specimens. Future studies of this specimen should further evaluate the nonlinear behavior of its anticlastic curvature, should account for delamination closure near its edges, and should focus on curved delamination fronts like those observed in tests.

References

[1]Wang, S. S., Mandell, J. F., and McGarry, F. J., "An Analysis of the Crack Tip Stress Field in DCB Adhesive Fracture Specimens," *International Journal of Fracture,* Vol. 14, No. 1, 1978, pp. 39–58.

[2]Crews, J. H., Jr., Shivakumar, K. N., and Raju, I. S., "Factors Influencing Elastic Stresses in Double Cantilever Beam Specimens," *Adhesively Bonded Joints: Testing, Analysis, and Design*, edited by W. S. Johnson, American Society for Testing and Materials, Philadelphia, PA, ASTM STP 981, 1988, pp. 119–132.

[3]Russell, A. J., "Factors Affecting the Opening Mode Delamination of Graphite/Epoxy Laminates," Defence Research Establishment Pacific, Dept. of Natural Defence, Materials Rept. 82-Q, Victoria, BC, Canada, Dec. 1982.

[4]Schapery, R. A., Goetz, D. P., and Lamborn, M. J., "Damage Models for Delamination and Transverse Fracture," Texas A&M Univ., College Station, TX, Rept. 5034-87-11, 1987.

[5]Davidson, B. D., "Two New Techniques for Predicting Delamination Growth in Laminated Plates," Ph.D. Dissertation, Texas A&M Univ., Dec. 1988.

[6]Davidson, B. D., and Schapery, R. A., "Effect of Finite Width on Deflection and Energy Release Rate of an Orthotropic Double Cantilever Specimen," *Journal of Composite Materials*, Vol. 22, July 1988, pp. 640–656.

[7]Raju, I. S., Shivakumar, K. N., and Crews, J., Jr., "Three-Dimensional Elastic Analysis of a Composite Double Cantilever Beam Specimen," *AIAA Journal*, Vol. 26, No. 12, 1988, pp. 1493–1498.

[8]Ashwell, D. G., "The Anticlastic Curvature of Rectangular Beams and Plates," *Journal of the Royal Aeronautical Society*, Vol. 54, 1950, pp. 708–715.

[9]Hyer, M. W., and Bhavani, P. C., "Suppression of Anticlastic Curvature in Isotropic and Composite Plates," *International Journal of Solids and Structures*, Vol. 20, No. 6, 1984, pp. 553–570.

[10]Shivakumar, K. N., Tan, P. W., and Newman, J. C., Jr., "A Virtual Crack-Closure Technique for Calculating Stress Intensity Factors for Cracked Three Dimensional Bodies," *International Journal of Fracture*, Vol. 36, 1988, pp. R43–R50.

[11]Shivakumar, K. N., and Raju, I. S., "Treatment of Singularities in Cracked Bodies," *International Journal of Fracture*, Vol. 45, 1990, pp. 159–176.

[12]Crews, J. H., Jr., and Reeder, J. R., "A Mixed-Mode Bending Apparatus for Delamination Testing," NASA TM-100662, Aug. 1988.

[13]Hartranft, R. J., and Sih, G. C. "The Use of Eigenfunction Expansions in the General Solution of Three-Dimensional Crack Problems," *Journal of Mathematics and Mechanics*, Vol. 19, No. 2, 1969, pp. 123–138.

[14]Tracey, D. M., "Finite Elements for Determination of Crack Tip Elastic Stress Intensity Factors," *Eng. Fract. Mech.*, Vol. 3, Oct. 1971, pp. 255–265.

[15]Raju, I. S., and Newman, J. C., Jr., "Three-Dimensional Finite Element Analysis of Finite-Thickness Fracture Specimens," NASA TN D-8414, May 1977.

[16]Raju, I. S., and Newman, J. C., Jr., "Stress-Intensity Factors for Corner Cracks in Rectangular Bars," *Fracture Mechanics: Nineteenth Symposium*, edited by T. A. Cruse, American Society for Testing and Materials, Philadelphia, PA, ASTM TP 969, 1988, pp. 43–55.

[17]Johnson, W. S., and Mangalgiri, P. D., "Investigation of Fiber Bridging in Double Cantilever Beam Specimens," *Journal of Composites Technology and Research*, Vol. 9, No. 1, 1987, pp. 10–13.